WHERE DOES FLUID-LIKE TURBULENCE BREAK DOWN IN THE SOLAR WIND?

S. Perri[1], V. Carbone[2], AND P. Veltri[2]
[1] International Space Science Institute, Hallerstrasse 6, Bern, CH-3012, Switzerland; silvia.perri@issibern.ch
[2] Dipartimento di Fisica, Università della Calabria–Via P. Bucci 31/C, I-87036 Rende, Italy

ABSTRACT

Power spectra of the magnetic field in solar wind display a Kolmogorov law $f^{-5/3}$ at intermediate range of frequencies f, say within the inertial range. Two spectral breaks are also observed: one separating the inertial range from an f^{-1} spectrum at lower frequencies, and another one between the inertial range and an $f^{-7/3}$ spectrum at higher frequencies. The breaking of fluid-like turbulence at high frequencies has been attributed to either the occurrence of kinetic Alfvén wave fluctuations above the ion-cyclotron frequency or to whistler turbulence above the frequency corresponding to the proton gyroradius. Using solar wind data, we show that the observed high-frequency spectral break seems to be independent of the distance from the Sun, and then of both the ion-cyclotron frequency and the proton gyroradius. We suppose that the observed high-frequency break could be either caused by a combination of different physical processes or associated with a remnant signature of coronal turbulence.

Key words: interplanetary medium – turbulence

1. INTRODUCTION

Since the first spacecraft observations the solar wind has shown properties typical of a plasma in a high turbulent state (Tu & Marsch 1995; Bruno & Carbone 2005). Plasma turbulence is characterized by a magnetic spectrum, at intermediate frequencies, following a power law $f^{-5/3}$, which has been attributed to a Kolmogorov-like turbulent energy cascade (Bruno & Carbone 2005; Sorriso-Valvo et al. 2007). Lower frequencies are characterized by a flicker noise f^{-1} spectrum, probably due to residual uncorrelated coronal structures (Matthaeus et al. 2007; Telloni et al. 2009). At high frequencies, the spectrum of magnetic field fluctuations shows a power law $f^{-\alpha}$ with a steeper slope $\alpha \in [2, 4]$, the average value being close to $\alpha \simeq 7/3$ (Leamon et al. 1998; Smith et al. 2006; Alexandrova et al. 2008). The origin of the high-frequency part of the spectrum has been either associated with a dissipative range, as in non-magnetized fluids (Leamon et al. 1998, 1999, 2000; Bale et al. 2005; Smith et al. 2006), or with a different turbulent energy cascade (Alexandrova et al. 2008; Ghosh et al. 1996; Stawicki et al. 2001; Li et al. 2001) caused by dispersive effects (Biskamp et al. 1996; Sahraoui et al. 2006, 2009; Servidio et al. 2007; Galtier & Buchlin 2007).

The scale where the magnetic energy spectrum described by a Kolmogorov law breaks down is a matter of discussion and strongly depends on the mechanism which is supposed to be the onset of the high-frequency region. Two competing processes have been proposed in literature considering that the Alfvénic low-frequency energy cascade (Sorriso-Valvo et al. 2007; Smith et al. 2009; Carbone et al. 2009) continues toward the high-frequency region. In a first scenario, Alfvénic modes at high frequencies are suppressed by proton cyclotron damping, and the cascade is basically due to weakly damped whistler modes, which generate a dispersive region (Stawicki et al. 2001; Li et al. 2001). From this point of view the spectral breakpoint scales as the inverse of the proton inertial length, c/ω_p (being ω_p the proton plasma frequency). According to a different scenario (Howes et al. 2008; Schekochihin et al. 2009), the cascade continues through perpendicularly propagating kinetic Alfvén waves, giving rise to a dispersive range. In this case, the spectral breakpoint scales as the proton gyroradius

v_{th}/ω_{ci} (being v_{th} and ω_{ci} the proton thermal speed and the ion gyrofrequency, respectively). At 1 AU, the high-frequency spectral break results to be close to both those characteristic scales, thus making difficult to validate one model instead of the other one. Both the scenarios are based on the presence of "modes," thus underlining the presence of weak turbulence at high frequencies. As a different approach the dispersive region could be generated by a different energy cascade of strong turbulence (Servidio et al. 2007; Alexandrova et al. 2008). Numerical simulations of compressible Hall MHD show that a spectral break exists at scales of the order of the ion-skin depth, where the Alfvénic turbulence breaks down giving place to a new kind of turbulence, called magnetosonic turbulence, characterized by fluctuations of density anti-correlated with magnetic field fluctuations traveling perpendicularly to the mean magnetic field (Servidio et al. 2007). Through Hall turbulence, phenomenological arguments can be used to easily reproduce the $f^{-7/3}$ spectral slope (Alexandrova et al. 2008).

The problem of the determination of the spectral break is urgent to establish which physical mechanism is responsible for the observed high-frequency spectrum. Therefore, in the present Letter, we investigate the radial evolution of the spectral break using high-resolution data from the *Ulysses* spacecraft in the outer heliosphere (i.e., $R > 1$ AU) and from the recent *MESSENGER* mission in the inner heliosphere (i.e., $R < 1$ AU), showing that the high-frequency kink does not scale as the characteristic plasma frequencies.

2. DATA ANALYSIS AND RESULTS

We analyze several solar wind streams spanning the range 0.3–5 AU. In the inner heliosphere, we have analyzed 1 day intervals using the 2 Hz sampled data from the MAG experiment on board the *MESSENGER* spacecraft (Anderson et al. 2007) during periods in which the satellite was in the interplanetary space. All the data sets here shown are in the Radial–Tangential–Normal reference frame. In the outer heliosphere, we have studied fast wind stream periods using the 1 s resolution magnetic field data from the MAG instrument on board *Ulysses* (Balogh et al. 1992). Each of those time intervals includes roughly 4 days. Radial distance, heliolatitude

Table 1
List of Parameters Relevant to the Data Sets Analyzed

Interval	R (AU)	θ (°)	B (nT)	V_{sw} (km s^{-1})	T_p (eV)
2009, 280	0.3		22.0		
2009, 185	0.5		10.7		
1995, 12–15	1.5	36 S	3.03	690	17.4
1994, 274–277	2.0	78 S	1.55	779	17.1
1994, 182–185	2.8	71 S	0.99	805	15.9
1994, 28–31	3.7	51 S	0.70	730	11.7
1996, 180–183	4.0	31 N	0.59	748	13.1
1993, 275–278	4.2	40 S	0.59	752	14.6
1993, 82–85	4.9	27 S	0.54	742	14.6

Note. Col. 2: radial distance; Col. 3: heliolatitude; Col. 4: magnetic field intensity; Col. 5: bulk speed; Col. 6: proton temperature.

θ, and magnetic field magnitude are listed in Table 1 for all the time intervals. Some plasma parameters from the SWOOPS experiment on board *Ulysses* (Bame et al. 1992) are also displayed; unfortunately, plasma parameters are not available from *MESSENGER*. The *Ulysses* data sets show a high proton speed as well as a very low coronal temperature (not listed), the latter being determined by the oxygen O^{7+}/O^{6+} ratio (Geiss et al. 1995); these are characteristic signatures of the solar wind coming from coronal holes which exhibits reasonably good stationarity conditions (Perri & Balogh 2010). The average values of the O^{7+}/O^{6+} ratio have been found to be roughly $\leqslant 10^{-1}$. Since we are dealing with time series coming from single spacecraft observations, we compute the magnetic field power spectra as a function of frequency, $f = 1/\tau$, with τ indicating a timescale, under the hypothesis that this is equivalent to compute the spectra as a function of the wavevector component along the flow direction, namely, $k = 2\pi f/V_{sw}$, being the solar wind bulk speed the transformation parameter. It is worth remarking that the *MESSENGER* spacecraft is in the ecliptic and that it only observes mixed solar wind streams; therefore we have analyzed time intervals of 1 day period in order to minimize the presence of shocks and transitions between different wind conditions.

Figure 1 shows the power spectral density (PSD) of the magnetic field, computed as the trace of the spectral matrix of **B**, for the time periods 2009 day 185 (left panel) by using *MESSENGER* data, and for the time interval in 1995 days 12–15 from the *Ulysses* spacecraft (right panel) in log–log scale. We have used a multitaper technique which estimates each spectrum as the average of K eigenspectra computed over spectral windows determined by a set of orthogonal data tapers (Percival & Walden 1993). This method reduces bias problems as it uses the full data length. In the PSD displayed in the right panel in Figure 1, it is possible to recognize the three different regions which characterize the magnetic field power spectra, that is the low-frequency range, $f \in [10^{-6}, 5 \times 10^{-4}]$ Hz (hereafter RANGE1), the intermediate range $f \in [10^{-3}, 10^{-1}]$ Hz (hereafter RANGE2), and the high-frequency range roughly observed for $f > 10^{-1}$ Hz (hereafter RANGE3). For comparison, along with both the low- and the high-frequency spectral breaks, namely, f_1 and f_2, indicated by vertical black dashed lines, the characteristic frequencies, that is the Doppler-shifted ion-cyclotron frequency, f_{ci}, the frequencies corresponding to the proton gyroradius ρ_p, namely, f_ρ, and to the proton inertial length $\lambda_p = c/\omega_p$, i.e., f_λ, are also displayed (see Figure 1).

The three scalings have been fitted with linear relationships; the power spectra spectral slopes obtained from the fits are
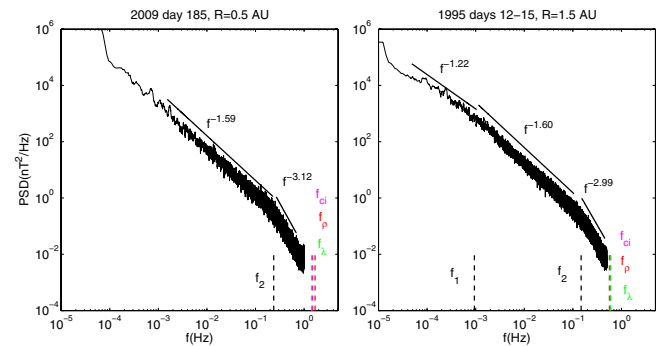

Figure 1. PSD of the magnetic field at 0.5 AU (left panel) computed from the *MESSENGER* data and the one at 1.5 AU (right panel) from the *Ulysses* data set. Both the low- and high-frequency breaks are indicated (vertical black dashed lines), along with plasma characteristic frequencies (see the text). The typical low-, intermediate- and high-frequency ranges are well recognizable.

Table 2
Slopes for the Best Power-law Fits in the Three Ranges of the Magnetic Field PSD for the Data Sets at Different R

R (AU)	RANGE1	RANGE2	RANGE3
0.3		1.626 ± 0.005	2.347 ± 0.006
0.5		1.587 ± 0.002	3.117 ± 0.007
1.5	1.22 ± 0.02	1.604 ± 0.002	2.992 ± 0.003
2.0	1.14 ± 0.04	1.696 ± 0.001	3.022 ± 0.004
2.8	1.22 ± 0.04	1.728 ± 0.004	3.476 ± 0.004
3.7	1.43 ± 0.06	1.697 ± 0.002	2.955 ± 0.004
4.0	1.05 ± 0.04	1.745 ± 0.002	3.167 ± 0.004
4.2	1.39 ± 0.06	1.644 ± 0.002	2.823 ± 0.003
4.9	1.3 ± 0.2	1.726 ± 0.002	2.36 ± 0.01

reported in Table 2 for all the periods analyzed. From a comparison of the values of the spectral slopes in RANGE2 computed from the *Ulysses* time series (see Table 2) and the values of the proton temperature reported in Table 1, we can confirm that the inertial range becomes steeper as T_p decreases (Belcher & Davis 1971; Leamon et al. 1998) for roughly all the data sets shown. Further, Leamon et al. (1998) found the opposite behavior for the spectral slope in the high-frequency range; that is, high proton temperature intervals have a steeper high-frequency spectrum (which implies a greater heating rate). However, the values of the spectral slopes shown in Table 2 for the RANGE3 do not exhibit a clear trend.

The positions of both the low-frequency break, f_1, and the high-frequency break, f_2, have been obtained from the intersection of the two best-fit power laws. Their values are displayed in Table 3 for all the data sets analyzed. As expected, f_1 moves significantly to lower frequencies as the radial distance increases (there is only an exception for the 1994 days 182–185 interval), meaning that the inertial range tends to be extended over a wider frequency range (Bavassano et al. 1982; Klein et al. 1992; Feynmann et al. 1996). This has been interpreted as due to the decay of low-frequency $1/f$ fluctuations originated close to the Sun into the higher frequency range, which happens at larger scales as the radial distance increases (Matthaeus & Goldstein 1986). Note that the intervals in the outer heliosphere here considered represent high latitude (i.e., $\theta > 30°$N/S) fast wind streams, characterized by a lack of shears and stream structures, which are instead typical of low latitude wind. This does not prevent the turbulent evolution of magnetic field fluctuations (Horbury et al. 1996; Sorriso-Valvo et al. 2007).

A clear trend is not observed for the high-frequency break. In the left panel in Figure 2 the values of f_2 (blue circles),

Table 3
Low- and High-frequency Breakpoint Positions for the Time Intervals Studied
as a Function of the Distance from the Sun

R (AU)	f_1 (Hz)	f_2 (Hz)
0.3		0.26 ± 0.01
0.5		0.237 ± 0.005
1.5	$(0.94 \pm 0.47) \times 10^{-3}$	0.148 ± 0.002
2.0	$(0.67 \pm 0.27) \times 10^{-3}$	0.160 ± 0.002
2.8	$(0.88 \pm 0.40) \times 10^{-3}$	0.140 ± 0.002
3.7	$(0.51 \pm 0.24) \times 10^{-3}$	0.120 ± 0.002
4.0	$(0.49 \pm 0.25) \times 10^{-3}$	0.140 ± 0.002
4.2	$(0.12 \pm 0.07) \times 10^{-3}$	0.140 ± 0.003
4.9	$(0.42 \pm 0.16) \times 10^{-3}$	0.090 ± 0.009

Figure 2. High-frequency spectral break f_2 (blue empty circles) and the Doppler-shifted ion-cyclotron frequency (black asterisks) as a function of the radial distance R (left panel). High-frequency spectral break (blue empty circles), the frequencies corresponding to the proton gyroradius (red crosses) and the proton inertial length (green $\times$) as a function of R, and the best fits of the radial trend of f_ρ (solid line) and of f_λ (dashed line, right panel) are shown. Error bars for the spectral break positions are also shown.

found from the intersection between the best power-law fit in the inertial range and the one in the high-frequency range, are plotted as a function of R along with the Doppler-shifted ion-cyclotron frequency, f_{ci}, (black asterisks). Further, error bars of the break estimation are also shown, they have been computed via the propagation of uncertainty. At $R = 0.3$ and $R = 0.5$ AU, we have estimated the Doppler shift by using 1 hr resolution *Helios 2* plasma data at those heliocentric distances within time intervals of high speed streams (in order to minimize the effects of variability). While, as expected, the Doppler-shifted ion-cyclotron frequency scales with R because it is proportional to the magnetic field intensity, which decreases as the radial distance increases (Jokipii & Kota 1989), the breakpoint frequency does not show any remarkable evolution, being confined in a short frequency range. In the right panel of Figure 2, the high-frequency spectral break position is displayed along with the frequencies corresponding to the proton gyroradius (red crosses) and to the proton inertial length (green $\times$). Again, their frequencies are well separated from f_2. Our results clearly show that, even if the amplitude of the frequency break f_2 is rather close to characteristic plasma frequencies, their radial scaling is completely different, say f_2 seems to be independent of the single frequencies.

3. DISCUSSION AND CONCLUSIONS

The results of our analysis reveal a problem with the interpretation of the physical processes which have been supposed to explain the presence of the high-frequency region of the solar wind turbulence. As we mentioned above, the break of fluid-like turbulence in the solar wind has been related to different processes involving characteristic frequencies, as the ion-cyclotron frequency and the ones associated with the ion inertial length and with the proton gyroradius. A comparison between the scalings of both the characteristic frequencies and the observed spectral break should allow us to tentatively discriminate among the various physical mechanisms. At variance to these claims, our results show that, while all the characteristic plasma frequencies exhibit a clear radial trend because of their dependence on the magnetic field and on some plasma parameters, the high-frequency break remains roughly constant as the distance from the Sun increases.

In Markovskii et al. (2008), a statistical analysis of the high-frequency spectral break have been performed using data coming from the *ACE* spacecraft at a single distance of about 1 AU. The frequency of the break has been found to be affected by different plasma parameters. By using high-resolution *MESSENGER* data from solar wind during time intervals characterized by different values of the intensity of the interplanetary
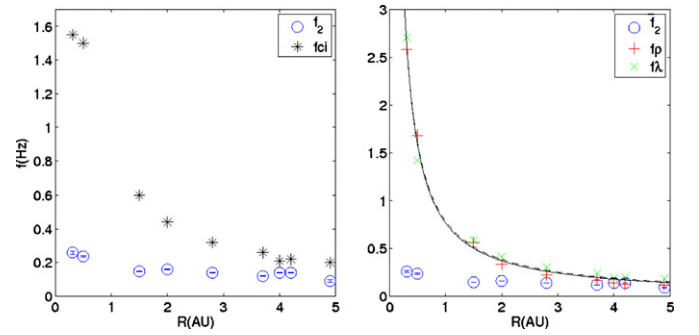
magnetic field, Korth et al. (2010) have found a slight dependence of the high-frequency break position on the magnetic field strength. The data used in the inner heliosphere come from the solar wind in the ecliptic where a high variability is routinely observed and a clear separation between RANGE2 and RANGE3 is not always identified. This is the origin of the slight difference between $R < 1$ AU and $R > 1$ AU. It can be concluded that the position of the break at 1 AU is not determined by the scaling of a single plasma parameter, but rather by a nonlinear combination of their scales and of their amplitudes at a given scale (Markovskii et al. 2008). Looking at our results, this might be extended throughout the whole heliosphere. Let suppose that the frequency position of the spectral break f_2 is a function of the characteristic frequencies defined above, that is $f_2 = g(f_\rho, f_\lambda)$. Let now generalize the radial dependence of the proton temperature, of the proton density, and of the solar wind magnetic field as $T_p \sim R^{-\beta}$, $n_p \sim R^{-\gamma}$, and $B \sim R^{-\delta}$, respectively. This implies that the proton gyroradius scales as $\rho_p \sim \sqrt{2T_p}/B \sim R^{-\beta/2+\delta}$, while the proton inertial length scales as $\lambda_p \sim 1/\sqrt{n_p} \sim R^{\gamma/2}$. This means that the characteristic frequencies scale as $f_\rho \sim R^{\beta/2-\delta}$ and $f_\lambda \sim R^{-\gamma/2}$. Through a fit on the data, shown in the right panel of Figure 2, we obtain the best-fit radial trends $f_\rho \sim R^{-1.05}$ (solid line) and $f_\lambda \sim R^{-1.03}$ (dashed line). Since we can imagine a nonlinear combination of the two characteristic frequencies as, for example, $f_2 \sim f_\rho^\eta f_\lambda^\mu$, it is possible to conjecture the simplest possible relation

$$f_2 = \frac{f_\rho^2}{f_\lambda} \sim \frac{\lambda_p}{\rho_p^2} \sim R^{\beta - 2\delta + \gamma/2}, \qquad (1)$$

which results to be independent of R only when $\beta - 2\delta + \gamma/2 = 0$. From the best-fit parameters, we obtain $\gamma \simeq 2$ in agreement with direct spacecraft observations (Belcher et al. 1993) and $\delta - \beta/2 \simeq 1.05$. Assuming a typical exponent for the radial trend of the proton temperature $\beta \simeq 1$ (Phillips et al. 1995), the exponent for the magnetic field results to be $\delta \simeq 1.55$. This is a reasonable value within a range of heliocentric distances 0.3–5 AU, because the radial component of the magnetic field scales as $1/R^2$, while their transverse components scale as $1/R$ (Jokipii & Kota 1989). At large radial distances we expect a prevailing $1/R$ trend for the magnetic field, because their radial component decreases faster than the tangential and the normal ones. The large-distance behavior can also be reproduced by the conjecture in Equation (1). Indeed, assuming $\beta = 1$ and $\gamma = 2$,

Equation (1) results to be independent of R if $\delta = \beta/2 + \gamma/4 = 1$. From a theoretical point of view, our finding and the practical impossibility of distinguishing different mechanisms, which should be at the origin of the high-frequency spectrum, lead to the conclusion that all modes can probably contribute to the high-frequency spectrum (Gary & Smith 2009). It is worth noticing that different simple functional shapes, as, for example, $f_2 = f_\lambda^2/f_\rho$ or $f_2 = (f_\lambda f_\rho)^{1/2}$, give rise to disagreements with observations of the radial decrease of the magnetic field.

Another explanation of the independence of the frequency break of R could be that the processes responsible for the onset of the high-frequency range are not evolving with R and depend upon neither the intensity of the magnetic field nor upon the local plasma parameters. This is based on the simple fact that turbulence in the solar wind is frozen after the Alfvénic point near the Sun and that, therefore, the spectral break could represent a coronal imprint. Measurements of spectral profiles show that turbulence starts to develop while passing from the photosphere to the chromosphere of the Sun (Reardon et al. 2008). Even if we do not have direct access to turbulence in the external solar corona, we can reasonably conjecture that the nonlinear energy cascade is responsible for the generation of a power spectrum of magnetic energy up to a certain frequency f_2. After the Alfvénic point, fluctuations are transported with the super-Alfvénic and supersonic solar wind with a weak residual evolution at small scales. In addition, measurements of the electric field in the solar wind could help to understand the nature of the high-frequency spectral break. Indeed, numerical simulations of Hall MHD turbulence (Dmitruk & Matthaeus 2006) have shown that the Hall term affects the electric field power spectrum at scales smaller than the ion-skin depth (close to the dissipation range), while it has no effects on the magnetic and velocity field power spectra. However, large statistics on measurements in the inner heliosphere is crucial to better assess this issue. New measurements will become available once the planned *Solar Orbiter* spacecraft is launched.

REFERENCES

Alexandrova, O., Carbone, V., Veltri, P., & Sorriso-Valvo, L. 2008, ApJ, 674, 1153
Anderson, B. J., Acuña, M.-H., Lohr, D.-A., Scheifele, J., Raval, A., Korth, H., & Slavin, J.-A. 2007, Space Sci. Rev., 131, 417
Bale, S.-D., Kellog, P.-J., Mozer, F.-S., Horbury, T.-S., & Reme, H. 2005, Phys. Rev. Lett., 94, 215002
Balogh, A., Beek, T.-J., Forsyth, R.-J., Hedgecock, P.-C., Marquedant, R.-J., Smith, E.-J., Southwood, D.-J., & Tsurutani, B.-T. 1992, A&AS, 92, 221
Bame, S.-J., McComas, D.-J., Barraclough, B.-L., Phillips, J.-L., Sofaly, K.-J., Chavez, J.-C., Goldstein, B.-E., & Sakurai, R.-K. 1992, A&AS, 92, 237
Bavassano, B., Dobrowolny, M., Mariani, F., & Ness, N.-F. 1982, J. Geophys. Res., 87, 3617
Belcher, J.-W., & Davis, L., Jr. 1971, J. Geophys. Res., 76, 3534
Belcher, J.-W., Lazarus, A.-J., McNutt, R.-L., Jr., & Gordon, G.-S., Jr. 1993, J. Geophys. Res., 98, 15177
Biskamp, D., Schwarz, E., & Drake, J.-F. 1996, Phys. Rev. Lett., 76, 1264
Bruno, R., & Carbone, V. 2005, Living Rev. Solar. Phys., 2, 4
Carbone, V., Marino, R., Sorriso-Valvo, L., Noullez, A., & Bruno, R. 2009, Phys. Rev. Lett., 103, 061102
Dmitruk, P., & Matthaeus, W.-H. 2006, Phys. Plasmas, 13, 042307
Feynman, J., Ruzmaikin, A.-A., & Smith, E.-J. 1996, in AIP Conf. Proc. 382, Solar Wind Eight, ed. D. Winterhalter et al. (Melville, NY: AIP), 347
Galtier, S., & Buchlin, E. 2007, ApJ, 656, 560
Gary, P., & Smith, C.-W. 2009, J. Geophys. Res., 114, A12105
Geiss, J., Gloecker, G., & von Steiger, R. 1995, Space Sci. Rev., 72, 49
Ghosh, S., Siregar, E., Roberts, D.-A., & Goldstein, M.-L. 1996, J. Geophys. Res., 101, 2493
Horbury, T.-H., Balogh, A., Forsyth, R.-J., & Smith, E.-J. 1996, A&A, 316, 333
Howes, G.-G., Dorland, W., Cowley, S.-C., Hammett, G.-W., Quataert, E., Schekochihin, A.-A., & Tatsuno, T. 2008, Phys. Rev. Lett., 10, 065004
Jokipii, J.-R., & Kota, J. 1989, Geophys. Res. Lett., 16, 1
Klein, L.-W., Matthaeus, W.-H., Roberts, D.-A., & Goldstein, M. L. 1992, in Conf. Proc.: Solar Wind Seven, ed. E. Marsch & R. Schwenn (Oxford: Pergamon), 197
Korth, H., et al. 2010, Planet. Space Sci., in press
Leamon, R. J., Matthaeus, W.-H., Smith, C.-W., Zank, G.-P., Mullan, D.-J., & Oughton, S. 2000, ApJ, 537, 1054
Leamon, R.-J., Smith, C.-W., Ness, N.-F., Matthaeus, W.-H., & Wong, H.-K. 1998, J. Geophys. Res., 103, 4775
Leamon, R.-J., Smith, C.-W., Ness, N.-F., & Wong, H.-K. 1999, J. Geophys. Res., 104, 22331
Li, H., Gary, S.-P., & Stawicki, O. 2001, Geophys. Res. Lett., 28, 1347
Markovskii, S.-A., Vasquez, B.-J., & Smith, C.-W. 2008, ApJ, 675, 1576
Matthaeus, W.-H., Breech, B., Dmitruk, P., Bemporad, A., Poletto, G., Velli, M., & Romoli, M. 2007, ApJ, 657, L121
Matthaeus, W.-H., & Goldstein, M.-L. 1986, Phys. Rev. Lett., 57, 495
Percival, D.-B., & Walden, A.-T 1993, Spectral Analysis for Physical Applications (Cambridge: Cambridge Univ. Press)
Perri, S., & Balogh, A. 2010, ApJ, 714, 937
Phillips, J.-L., Bame, S.-J., Gary, S.-P., Gosling, J.-T., Scime, E.-E., & Forsyth, R.-J. 1995, Space Sci. Rev., 72, 109
Reardon, K., Lepreti, F., Carbone, V., & Vecchio, A. 2008, ApJ, 683, L207
Sahraoui, F., Belmont, G., Rezeau, L., Cornilleau-Wehrlin, N., Pinçon, J.-L., & Balogh, A. 2006, Phys. Rev. Lett., 96, 075002
Sahraoui, F., Goldstein, M.-L., Robert, P., & Khotyaintsev, Y.-V. 2009, Phys. Rev. Lett., 102, 231102
Schekochihin, A.-A., Cowley, S.-C., Dorland, W., Hammett, G.-W., Howes, G.-G., Quataert, E., & Tatsuno, T. 2009, ApJS, 182, 310
Servidio, S., Carbone, V., Primavera, L., Veltri, P., & Stasiewicz, K. 2007, Planet. Space Sci., 55, 2239
Smith, C.-W., Hamilton, K., Vasquez, B.-J., & Leamon, R.-J. 2006, ApJ, 645, L85
Smith, C.-W., Stawarz, J.-E., Vasquez, B.-J., Forman, M.-A., & MacBride, B.-T. 2009, Phys. Rev. Lett., 103, 201101
Sorriso-Valvo, L., et al. 2007, Phys. Rev. Lett., 99, 115001
Stawicki, O., Gary, S.-P., & Li, H. 2001, J. Geophys. Res., 106, 8273
Telloni, D., Bruno, R., Carbone, V., Antonucci, E., & D'Amicis, R. 2009, ApJ, 706, 238
Tu, C.-Y., & Marsch, E. 1995, Space Sci. Rev., 73, 1